

Combinatorial drug screening identifies Ewing sarcoma-specific sensitivities

Branka Radic-Sarikas¹, Kalliopi P. Tsafou^{2,6}, Kristina B. Emdal³, Theodore Papamarkou⁴, Kilian V. M. Huber¹, Cornelia Mutz⁵, Jeffrey A. Toretsky⁶, Keiryn L. Bennett¹, Jesper V. Olsen³, Søren Brunak², Heinrich Kovar^{5,7} and Giulio Superti-Furga^{1,8,*}

¹CeMM Research Center for Molecular Medicine of the Austrian Academy of Sciences, Vienna, Austria.

²Center for Biological Sequence Analysis, Department of Systems Biology, Technical University of Denmark, Lyngby, Denmark.

³Proteomics Program, Novo Nordisk Foundation Center for Protein Research, Faculty of Health and Medical Sciences, University of Copenhagen, Copenhagen, Denmark.

⁴School of Mathematics and Statistics, University of Glasgow, Glasgow, United Kingdom.

⁵Children's Cancer Research Institute, St. Anna Kinderkrebsforschung, Vienna, Austria.

⁶Department of Oncology, Georgetown University Medical Center, Washington, DC, USA.

⁷Department of Pediatrics, Medical University, Vienna.

⁸Center for Physiology and Pharmacology, Medical University of Vienna, Vienna, Austria.

Running title: Synergy screen for Ewing sarcoma-specific sensitivities

Key words: drug synergy, disease-specific, resistance, Ewing sarcoma, drug profiling

Abbreviations: EWS, Ewing sarcoma breakpoint region 1, at chromosome 22; ETS, E-twenty-six family; FLI1, Friend leukemia integration 1 transcription factor; INSR, insulin receptor; IGF1, Insulin-like growth factor 1; IGF1R, insulin-like growth factor 1 receptor; CI, combination index; MS, mass spectrometry; LC-MS, liquid chromatography–mass spectrometry; LC-MS/MS, liquid chromatography–tandem mass spectrometry; kd, knockdown.

Corresponding author: Prof. Dr. Giulio Superti-Furga
Scientific Director CeMM
gsuperti@cemm.oeaw.ac.at
M: +43-664-4042300
Fax: +43-1-40160-970000

Jeffrey A. Toretsky is reporting to have a minor ownership interest and to receive a major compensation as a consultant/advisory board member in Oncternal Therapeutics. Other authors disclose no potential conflicts of interest.

Funding: B. Radic-Sarikas, K.P. Tsafou, K.B. Emdal, T. Papamarkou, K.V.M. Huber, J.V. Olsen, S. Brunak, H. Kovar and G. Superti-Furga were funded by the European Union Seventh Framework Programme (FP7/2007- 2013) ASSET project under grant agreement number FP7- HEALTH-2010-259348-2. C. Mutz was funded by FWF ERA-Net grant I1225-B19. K.L. Bennett was supported by the Austrian Academy of Sciences.

Abstract

Improvements in survival for Ewing sarcoma pediatric and adolescent patients have been modest over the past 20 years. Combinations of anticancer agents endure as an option to overcome resistance to single treatments caused by compensatory pathways. Moreover, combinations are thought to lessen any associated adverse side effects through reduced dosing, which is particularly important in childhood tumors. Using a parallel phenotypic combinatorial screening approach of cells derived from three pediatric tumor types, we identified Ewing sarcoma -specific interactions of a diverse set of targeted agents including approved drugs. We were able to retrieve highly synergistic drug combinations specific for Ewing sarcoma and identified signaling processes important for Ewing sarcoma cell proliferation determined by EWS-FLI1. We generated a molecular target profile of PKC412, a multikinase inhibitor with strong synergistic propensity in Ewing sarcoma, revealing its targets in critical Ewing sarcoma signaling routes. Using a multilevel experimental approach including quantitative phosphoproteomics, we analyzed the molecular rationale behind the disease-specific synergistic effect of simultaneous application of PKC412 and IGF1R inhibitors. The mechanism of the drug synergy between these inhibitors is different from the sum of the mechanisms of the single agents. The combination effectively inhibited pathway crosstalk and averted feedback loop repression, in EWS-FLI1 dependent manner.

Introduction

Pediatric tumors are highly diverse regarding their cells of origin, clinical features and onset time. Childhood cancer is mainly a consequence of altered regulation of normal tissue development. Furthermore, in most childhood tumors only a few mutations have been found in genes that code for druggable targets, thus rendering it more difficult to design therapeutic strategies. Among solid pediatric tumors the overall survival rate for recurrent or metastatic disease is less than 30% and many childhood cancer survivors experience long-term effects as a consequence of treatment that severely reduce their quality of life (1). Other than neuroblastoma, the 5-year survival rates for pediatric and adolescent solid tumors have not changed over the past two decades, particularly true in case of pediatric and adolescent sarcomas (2). Ewing sarcoma is the second most common pediatric bone tumor but can develop in soft tissue as well (extra-skeletal Ewing sarcoma). The disease onset usually in adolescent years with peak occurrence between ages 10 and 20. A vast number of childhood tumors have quiet genomes, and Ewing sarcoma has one of the quietest of all (3). The *FET-ETS* fusion is the defining molecular feature, most commonly involving *EWSR1* and *FLI1* (4,5). *STAG2*, *CDKN2A* and *TP53* are the only other genes found to be affected in up to 20% of cases; the prognostic significance of these mutations remains controversial (3,6–8). The EWS-FLI1 fusion oncoprotein is a result of a chromosomal translocation t(11:22) between the central exons 5' portion of the *EWSR1* (*EWS*) gene (Ewing sarcoma breakpoint region 1, at chromosome 22) to the central exons and the DNA binding domain containing portion of an *ETS* (E-twenty-six) family gene, most commonly *FLI1* (Friend leukemia integration 1, chromosome 11). EWS-FLI1 is an aberrant transcription factor which is considered the main pathogenic driver of the disease (9) since ~85% Ewing sarcoma cases are characterized by its presence. EWS-FLI1 mediates malignant transformation and drives the target gene expression (10,11). Transcription factors are per se very challenging drug targets since they lack a druggable pocket; their functional domains are less structurally susceptible compared to the enzymatic ones. Moreover, it is difficult to directly modulate protein/DNA binding. Thus, current studies have mainly focused on targeting signaling pathways that regulate the activity of EWS-FLI1. Initial promising results coincided with the availability of compounds that target molecules associated with Ewing sarcoma progression, such as CDKs, pro-apoptotic proteins and certain tyrosine kinases, e.g. realization of the importance of ROR1 in metastatic disease (12). The contribution of IGF1R/Insulin receptor (IGF1R/INSR) signaling pathway to Ewing sarcoma neoplastic transformation is widely accepted (13,14). IGF1 (Insulin-like growth factor 1) is a growth factor deposited in the bone matrix, and it is no coincidence that the peak of occurrence of Ewing sarcoma coincides with accelerated growth in

puberty, where IGF1 plays a major role. IGF1, together with few other members of the same signaling axis, is induced by the EWS-FLI1 fusion protein (15). IGF1 stimulates IGF1R receptors and triggers growth and pro-survival pathways (PI3K and RAS), thus creating a perfect niche for malignant transformation of cells. Whereas the response to IGF1R inhibitors was dramatic in a certain number of patients, the overall rate was discouraging. The reported resistance to anti-IGF1R therapies is often caused by the activation of bypass pathways (16). The PI3K/AKT/mTOR pathway plays an important role in Ewing sarcoma progression, as in many other malignancies (17). Furthermore, the MAPK/ERK pathway is involved in regulation of cellular responses to diverse range of extracellular stimuli including mitogens, growth factors, and cytokines, making it an important target in the diagnosis and treatment of various cancers, including Ewing sarcoma (18). Changes in calcium-dependent signaling mechanisms are frequently altered and remodeled in cancer cells, including Ca^{2+} sensors and effectors, such as calmodulin (CAM) and the downstream targets, including CAM kinase (CAMK), calcineurin and protein kinase C (PKC). Although a number of potential molecular targets have been proposed for Ewing sarcoma, such as IGF1R and other receptor tyrosine kinases inhibitors, mTOR and certain EWS-FLI1 related targets, the therapeutic efficacy of their inhibition is still modest, due to the lack of biomarkers and drug resistance, which lead to rather disappointing clinical data (19). The occurrence of drug resistance could be prevented or partly delayed by applying the concurrent combination treatment. A synergistic drug combination is more potent than equally effective doses of its components (20), thus providing additional benefit to patient over a simple increase in single dosages.

In this study we used a parallel screening approach to contrast combinatorial screens in three pediatric tumor entities and to identify combinations of targeted agents that act highly synergistically in a signaling context specifically altered by EWS-FLI1 expression. A drug library focused on clinically relevant agents allowed us to discover combinations with a potential to be translated into clinical treatment. Preclinical studies are required to determine the pharmacodynamic interactions and appropriately adjust *in vivo* dosing regimens. However, a broader concentration range where synergistic effect is preserved offers a higher probability of achieving the desired plasma concentration. Thus, we focused on combinations that showed a robust synergy. In the context of Ewing sarcoma, defined by the presence and activity of the EWS-FLI1 fusion protein, we analyzed the molecular rationale behind the Ewing sarcoma -specific synergistic effect of simultaneous application of PKC412 and IGF1R inhibitors using a multi-pronged experimental approach. PKC412 (midostaurin) is an oral, multi-targeted kinase inhibitor, recently approved by the FDA for treatment of patients with FLT3-mutated acute myeloid leukemia (AML)

and in phase II trial for mast cell leukemia (MCL) and aggressive systemic mastocytosis (ASM). Moreover, PKC412 has been shown to induce apoptosis of Ewing sarcoma cells in vitro and in vivo (21). We implemented chemical proteomics to profile the PKC412 target spectrum in the context of Ewing sarcoma and investigated the molecular effects elicited by the simultaneous application with the IGF1R/INSR inhibitors. OSI-906 and BMS-754807 are oral, reversible ATP-competitive antagonists of insulin-like growth factor 1 receptor (IGF1R). Unlike anti-IGF1R monoclonal antibodies, they also block the insulin receptor and the hybrid dimers (IGF1R/INSR) which is advantageous in cancer treatment (22). Moreover, both OSI-906 and BMS-754807 are judged to be rather specific, with BMS-754807 shown to inhibit only a few other kinases although with markedly lower potency than IGF1R and INSR (23). We identified the signaling routes in Ewing sarcoma whose synchronous inhibition allowed achieving a potent elimination of tumor cells and effective surpassing of the induction of compensatory signaling pathways.

Materials and Methods

Viability assays

The individual drug effects were determined in proliferation assays using Cell Titer Glo (Promega Inc., Madison WI, USA). 4×10^3 cells were seeded in 96-well plates in triplicates and treated with drugs 24 h after. Serial dilutions in a range between 20 μ M and 0.05 μ M were applied for 72 hours. In case of knockdown of EWS-FLI1, the induction with doxycycline was started 24h prior to drug treatment and the cells were kept in doxycycline until the readout. IC50 values were determined by fitting a dose response curve to the data points using non-linear regression analysis utilizing the GraphPad Prism software.

Compounds

PKC412 was purchased from LC Laboratories (Woburn, MA, USA). OSI-906 and BMS-754807 were purchased from Active Biochem (Kowloon, Hong Kong) and Selleck Chemicals (Munich, Germany). List of all compounds included in the libraries with their respective manufacturers is provided in Supplementary Table S1. All compounds were dissolved in dimethyl sulfoxide (DMSO) as 10 mM or 5 mM stock solutions.

Determination of synergy and analysis of the screen

The combination index (CI), see (24), was used for quantification of synergistic, antagonistic or additive effects of each drug pair. In order to capture synergistic effect if present, we obtained duplicate matrices for each drug pair, positioned in different screening plates. Cell viability was measured across a range of dose levels for each drug pair without maintaining the ratio of dose levels constant. In its conventional terminology, a non-constant ratio experimental design has been deployed. Such an experimental setup has been selected for the purposes of attaining a broad screening across drug combinations and dose levels. The well-known implication of carrying out the experiment at non-constant dose ratio has been the lack of ability to simulate CI across varying dose levels to estimate a smooth dose-response curve. However, it has been possible to calculate CI for each combination data point under the non-constant ratio design. The evaluated CI has then been mainly employed for classifying drug pairs as synergistic or antagonistic with respect to CI cut-offs, thus allowing to detect drug combinations with non-additive signals. Estimating CI for a given drug pair at an observed point entails a two-step process. Initially, the kinetic order m and median effect dose D_m appearing in median-effect equation (1) are estimated for each single drug. The median-effect equation expresses as

$$\frac{f_a}{f_u} = \left(\frac{D}{D_m} \right)^m, \quad (1)$$

where the observables are the fraction of unaffected (viable) cells f_u and drug dose D , while $f_a = 1 - f_u$ is the fraction of affected (inhibited) cells. To apply equation (1) to a single drug, the f_a , f_u , and D values for that drug are taken into account across all drug pairs at the instances of zero dosage for the other drug in each pair. Equation (1) is then log-transformed, and simple linear regression is used for estimating m and D_m . The second step involves computing the combination index

$$CI = \frac{D_1}{(D_m)_1 \left(\frac{f_a}{f_u} \right)^{1-m_1}} + \frac{D_2}{(D_m)_2 \left(\frac{f_a}{f_u} \right)^{1-m_2}}, \quad (2)$$

where D_i , $(D_m)_i$ are the dose and estimated median dose for drug i , $i \in \{1, 2\}$, in the pair.

Apoptosis measurements

Adherent and floating cells were analyzed 24 hours after compound treatment with the AnnexinV Apoptosis Detection Kit APC (eBioscience, San Diego, USA). AnnexinV and DAPI (Sigma-Aldrich) staining were performed according to manufacturer's instructions and FACS Fortessa (BD) and the

Diva software (BD, Version) were used for quantification purposes. As a positive control, apoptosis was induced via camptothecin (1 μ M for 24h).

Colony formation assay

1 \times 10⁴ cells per well were seeded in six-well plates in triplicates. After 24 h treatment with DMSO (equal to the highest amount of compound dilution, maximum 0.2%) or compounds at combination concentrations were added and cells incubated at 37 °C, 5% CO₂ for 7–10 days. Medium was aspirated, cells were washed with PBS (Gibco), stained with crystal violet solution (0.5% in 6% glutaraldehyde) and left to dry overnight. For quantification of results, ultraviolet absorbance of crystal violet was determined at 570 nm following solubilization by 70% ethanol. Data were analyzed using the GraphPad Prism software (t-test, p=0.05).

Real-time PCR analysis

RNeasy Mini Kit (Qiagen) was used for the isolation of total RNA. Total RNA was quantified using NanoDrop spectrophotometer (Thermo) and cDNA was synthesized from 500 ng of RNA via reverse transcription using oligo(dT) primers and RevertAid Reverse Transcriptase (Fermentas). Quantitative PCR was carried out on a RotorGene RG-600 (Qiagen) PCR machine using the SensiMix SYBR kit (Bioline). Results were quantified using the 2^{- $\Delta\Delta C_t$} method, using GAPDH expression levels for normalization.

Cell culture

The SH-SY5Y, IMR5-75, and UW228 cell lines were received as generous gifts from Drs. Frank Westermann and Alexandre Arcaro (obtained in 2011). A673 and A673 EWS-FLI1 conditional knockdown cell lines were a kind gift from Dr. Javier Alonso (obtained in 1992 and 2007, respectively). TC252, TC32, RDES, STA-ET-7.1, STA-ET-7.2, STA-ET-2.1, STA-ET-2.2 and TC71 Ewing sarcoma cell lines were acquired by Dr. Heinrich Kovar (obtained in years 1992, 2005, 1992, 1992., 1992, 1991, 1991 and 2006, respectively). No authentication was done by the authors. A673 and UW228 cells were cultured in DMEM (Sigma) media containing 10% fetal bovine serum and 10 U mL⁻¹ penicillin/streptomycin (Gibco). SH-SY5Y, TC252 and IMR5-75 cells were cultured in RPMI 1640 (Sigma) media containing 10% fetal bovine serum and 10 U mL⁻¹ penicillin/streptomycin (Gibco). TC32, RDES, STA-ET-7.1, STA-ET-7.2, STA-ET-2.1, STA-ET-2.2 and TC71 were grown on fibronectin (Roche) coated plates, and kept in RPMI 1640 (Sigma) media containing 10% fetal bovine serum and 10 U mL⁻¹ penicillin/streptomycin (Gibco).

Cell stimulation and immunoblotting

Cells were cultured in complete medium and serum starved over night, when indicated. Upon the 2h drug treatment, cells were stimulated for 20 minutes with 15% serum media. In case of a knockdown of EWS-FLI, cells were treated with doxycycline (1 µg/mL) 72 hours before serum stimulation, unless otherwise stated. The following antibodies were used: rabbit anti-actin (AAN01) (Cytoskeleton, AAN01), mouse anti-tubulin (DM1A) (Abcam, ab7291), mouse GAPDH (Santa Cruz, sc-365062), rabbit phospho-Akt (Ser473) (Cell Signaling, 4060S), rabbit phospho-Akt (Thr308) (Cell Signaling, 2965), rabbit Akt (pan) (11E7) (Cell Signaling, 4685), rabbit phospho-p70 S6 kinase (Thr389) (Cell Signaling, 9234), rabbit p70 S6 kinase α (C-18) (Santa Cruz, sc-230), rabbit FLI1 (Novus, NB600-537), rabbit pIGF1R β (Tyr1135/1136)/IR β (Tyr 1150/1151) (Cell Signaling, 3024), rabbit IGF-I Receptor β Antibody (Cell Signaling, 3027), rabbit phospho-p44/42 MAPK (Erk1/2) (Thr202/Tyr204) (Cell Signaling, 4370), mouse Erk-1/2 (Sigma, M 5670).

Determination of intracellular drug levels via Multiple reaction-monitoring assay

2×10^5 cells were treated with drugs at 37 °C, as stated. Subsequently, cells were washed three times with ice-cold PBS and directly lysed in 300 µL 80% ice-cold methanol. Lysates were then cleared by centrifugation for 20 min at 4 °C at 16,000 g, and supernatants were used for the following quantifications by MS. Multiple reaction-monitoring settings were automatically generated for every compound using the IntelliStart software (Waters), and quantification was conducted on the basis of the intensity of three daughter ions.

Compound immobilization and affinity purification

Drug-affinity matrices were prepared as described previously (25). In brief, 25 nmol of compound was immobilized on 50 µL NHS-activated Sepharose 4 Fast Flow beads (GE Healthcare Bio-Sciences AB, Uppsala, Sweden). Affinity chromatography and elution were performed in duplicate as reported previously (26) using 10 mg total cell lysate as a protein input per replicate.

Solution tryptic digestion and peptide purification

After elution, enriched proteins were reduced with dithiothreitol, cysteine residues alkylated by incubation with iodoacetamide and the samples digested with modified porcine trypsin (Promega, Madison, WI). Five percent (and multiples thereof) of the digested samples were purified and concentrated by C18 reversed-phase material for subsequent duplicate analysis by gel-free one-dimensional liquid chromatography mass spectrometry (1D-LCMS). Details of the LCMS methodology are as previously described (27).

Protein identification in chemical proteomic experiment

Peak extraction and conversion of raw MS files into the mgf format for subsequent protein identification was performed with msconvert (ProteoWizard Library v2.1.2708). An initial database search was performed with broader mass tolerance to re-calibrate the mass lists for protein identification. Mascot (version 2.3.02, MatrixScience, London, UK) was used for the initial protein database search. Error tolerances on the precursor and fragment ions were ± 10 ppm and ± 0.6 Da, respectively, and the database search was limited to fully-tryptic peptides with maximum 1 missed cleavage site. Carbamidomethyl cysteine and methionine oxidation were set as fixed and variable modifications, respectively. Searches were performed against the human UniProtKB/SwissProt database v2014.07_20141023 (40,984 sequences including isoforms obtained from varsplic.pl (28) and appended known contaminants). The initial peptide identifications were used to deduce independent linear transformations for precursor and fragment masses that would minimize the mean square deviation of measured masses from theoretical. Re-calibrated mass list files were searched against the same human protein database by the Mascot and Phenyx (version 2.5.14, GeneBio SA, Geneva, Switzerland) search engines with narrower mass tolerances (± 4 ppm and ± 0.3 Da). To validate the proteins, Mascot and Phenyx output files were processed by internally-developed parsers. Proteins with ≥ 2 unique peptides above a score T1, or with a single peptide above a score T2 were selected as unambiguous identifications. Additional peptides for these validated proteins with score $> T3$ were also accepted. For Mascot searches, the following thresholds were used: T1=14, T2=40 and T3=10; Phenyx thresholds were set to 4.2, 4.75 and 3.5, respectively (P-value $< 10^{-3}$). The validated proteins retrieved by the two algorithms were merged, any spectral conflicts discarded and grouped according to shared peptides. A false discovery rate (FDR) of $< 1\%$ for protein identifications and $< 0.1\%$ for peptides (including the ones exported with lower scores) was determined by applying the same procedure against a database of reversed protein sequences.

Bioinformatic analysis of drug pulldown data

The specificity of the compound – protein interactions generated by the pull down experiment was assessed using the software SAINT (29)(version 2.4.0). Using the protein spectral counts as measurement of abundance, SAINT algorithm compares the protein spectral counts of the pull down experiment and the negative control as a measurement of differential abundance to calculate the probability of a bait-prey interaction to be true. The fold change of the spectral counts is based on computing the ratio of the median spectral counts with or without competition with free compound. To eliminate background contaminants the CRAPome database was used (30). CRAPome is a

repository of negative controls generated by previous proteomics experiments and calculates a score for the interaction data as 1- number of experiments the protein is found in the database/total number of experiments in the database. The protein interaction networks were created by using the STRING database (version 10). Experimentally obtained interactions were filtered and a confidence score threshold of 0.7 (high confidence) was required. Protein compound associations were extracted from the database STITCH (version 4.0). Interactions derived from experiments but also interactions extracted from other databases were used and a minimum threshold of STITCH confidence score of 0.7 (high confidence) was required. Enrichment analysis was performed using the Gene Set Enrichment Analysis (GSEA) tool and pathway annotation was based on the KEGG ontology database with an FDR cutoff of 0.05. For network visualization and further data integration we used the Cytoscape platform (version 3.2.1).

SILAC labeling and cell treatments

For quantitative MS-based phosphoproteomics, the A673 cell line was labeled in SILAC DMEM (PAA Laboratories GmbH) supplemented with 10% dialyzed fetal bovine serum (Sigma), respectively, 2 mM l-glutamine (Gibco), 1 mM sodium pyruvate (Gibco), penicillin (100 U/ml), and streptomycin (100 µg/ml) for at least 7 passages to ensure complete incorporation of amino acids. Three cell populations were obtained: one labeled with natural variants of the amino acids (light label; Lys0, Arg0) (Sigma), the second labeled with medium variants of amino acids {L-[2H4]Lys (+4) and L-[13C6]Arg (+6)} (Lys4, Arg6), and the third labeled with heavy variants of the amino acids {L-[13C6,15N2]Lys (+8) and L-[13C6,15N4]Arg (+10)} (Lys8, Arg10). Medium and heavy variants of amino acids were purchased from Cambridge Isotope Laboratories. Cells from light, medium and heavy SILAC conditions were starved by replacing complete SILAC medium with SILAC minimal medium without serum over night. Cells were pretreated for 2 hours with 75 nM (0.25 IC50) PKC412 and 18 nM (0.25 IC50) BMS-754807; alone or in combination and 0.1% DMSO was used as control. Then, cells were stimulated with serum for 20 minutes and lysed separately at 4°C in ice-cold modified RIPA buffer [50 mM tris-HCl (pH 7.5), 150 mM NaCl, 1 mM EDTA, 1% NP-40, 0.1% sodium deoxycholate with the addition of 5 mM β-glycerophosphate, 5 mM sodium fluoride, 1 mM sodium orthovanadate, and one Complete Protease Inhibitor Cocktail tablet (Roche) per 50 ml of solution].

Sample preparation for phosphoproteomic MS analysis

Proteins were precipitated overnight at -20°C using ice-cold acetone. The acetone-precipitated proteins were solubilized in denaturation buffer [6 M Guanidine-HCl, 100 mM tris (pH 8.5), 5 mM

Tris (2-carboxyethyl) phosphine and 10 mM chloroacetamide], heated at 99°C and sonicated. 12 mg of protein from each SILAC condition was mixed 1:1:1. Proteins were digested initially with endoproteinase Lys-C for 3 hours (Wako), diluted threefold with 25 mM tris buffer, and then digested with trypsin (modified sequencing grade, Sigma) overnight. Enzyme activity was quenched by acidification of the samples with trifluoroacetic acid (TFA). The peptide mixture was desalted and concentrated on a C18 Sep-Pak cartridge (Waters) and eluted with 50% acetonitrile. Peptide fractionation was performed with 6 mg of peptides by high-pH high-pressure liquid chromatography (HPLC) essentially as described in Batth et al 2014 (31). A total number of concatenated fractions was set to 10. From each fraction phosphopeptides were enriched by two sequential rounds of titansphere chromatography. Briefly, titanium dioxide (TiO₂) beads (5 µm, Titansphere, GL Sciences) were incubated with a solution of 2,5-dihydroxybenzoic acid (DHB) (20 mg/ml) (Sigma-Aldrich) in 80% ACN, 1% TFA for 30 min at room temperature. 2 mg of TiO₂-DHB beads was added to each fraction and incubated under rotation for 30 min at room temperature. The beads were washed with 30% acetonitrile, 1% TFA and transferred to a C8 stage tip. Beads were washed with 50% acetonitrile, 1% TFA followed by 80% acetonitrile, 1% TFA. The bound phosphopeptides were eluted directly into a 96-well plate by 5% NH₄OH followed by 10% NH₄OH, 25% ACN. The eluate was immediately concentrated in a SpeedVac at 45°C and acidified with 5% ACN, 1% TFA. Each sample was then desalted and concentrated on a C18 stage tip.

Liquid chromatography–tandem mass spectrometry in phosphoproteome analysis

Peptides from all samples were eluted from C18 stage tips using 40% ACN, 0.5% acetic acid before online nanoflow LC-MS/MS analysis. Peptide mixtures were analyzed using a nanoscale UHPLC system (EASY-nLC1000 system from Thermo Fisher Scientific) connected to a Q Exactive HF mass spectrometer (Thermo Fisher Scientific) through a nanoelectrospray ion source. Peptides were separated in a 15-cm analytical column (75-µm inner diameter) in-house packed with 1.9-µm reversed-phase C18 beads (ReproSil-Pur AQ, Dr. Maisch) with a 106-min gradient from 8 to 64% acetonitrile in 0.5% formic acid at a flow rate of 250 nl/min. Standard mass spectrometric parameters were as follows: spray voltage, 2 kV; no sheath and auxiliary gas flow, heated capillary temperature, 275°C; S-lens radio frequency level of 50%. Full-scan MS spectra [mass/charge ratio (m/z), 375 to 1500; resolution, 120,000 at m/z 200] were detected in the Orbitrap analyzer after accumulation of ions at 3e6 target value based on predictive AGC from the previous scan. For every full scan, the 7 most intense ions were isolated and fragmented (collision energy: 28%) by higher-energy collisional dissociation (HCD) with a fixed injection/fill time of 110 ms and 60,000 resolution. Finally, the dynamic exclusion was set to 40 s.

Mass spectrometry data analysis (phosphoproteomics)

MS raw files were analyzed using MaxQuant software version 1.5.3.6 supported by the Andromeda search engine. Data were searched against a concatenated target/decoy (forward and reversed) version of the complete human UniProt database including commonly observed contaminants such as porcine trypsin and bovine serum proteins. The mass tolerance was set to 6 ppm for peptide masses and 20 ppm for HCD fragment ion masses. Cysteine carbamidomethylation was searched as a fixed modification. Protein N-acetylation, N-pyroglutamine, deamidation of asparagine and glutamine, oxidized methionine, and phosphorylation of serine, threonine, and tyrosine were searched as variable modifications. Phosphorylation site localization probabilities were determined by MaxQuant using the PTM (post-translational modification) scoring algorithm (32,33). A false discovery rate (FDR) was set to < 1% for peptide and phosphorylation site identifications. Only peptides with an Andromeda score > 40 (unmodified and modified) were included in the total peptide list. Minimal peptide length was seven amino acids. Only peptides with a phosphorylation site localization probability of at least 0.75 (32) were included in the bioinformatic analyses. To identify phosphorylation sites with significantly regulated ratios, we compared the ratio distributions of all quantified phosphopeptides with all nonphosphorylated peptides that we expect not to change and therefore specify our technical variance. To determine the level of regulation, each treatment condition was considered an independent experiment and cutoffs for up- and down-regulation were set to allow for an estimated 5% false-positive rate based on the distribution of ratios of identified and quantified non-phosphorylated peptides. Thus, cutoffs were individually determined for treatment condition.

Results

A parallel combinatorial drug screen reveals distinct Ewing sarcoma specific drug-drug interactions

We selected an initial library of targeted agents that were either clinically approved or in clinical trials. The library was comprised of 33 targeted compounds representing the potential new lines of therapy in pediatric tumors (Supplementary Fig. S1, Supplementary Table S1). Our goal was to identify Ewing sarcoma specific drug-drug interactions and pinpoint signaling routes that ought to be perturbed simultaneously in order to achieve strong synergistic effect in cancer cells killing. The overview of the combinatorial screening design is shown in Fig 1A. First we determined drug

potencies in A673 Ewing sarcoma cell line and the two cell lines representative of different pediatric tumor entities – neuroblastoma SH-SY5Y cell line and medulloblastoma UW228 cell line. Since synergistic drug effect can vary with the concentrations, we used a factorial dilution matrix approach which enabled us to capture drug associations in detail (34) and to select for combinations spread across larger concentration range. Due to the rapid augmentation of the number of data points with every compound in a concentration matrix-based screening design where each drug is combined with another, we selected a small combinatorial sub-library of drugs that potently inhibited cancer cell growth in all three cell lines (a total of 18 compounds; Supplementary Fig. S1, Supplementary Table S1). Combinatorial effect was measured using the combination index (CI) method (35) which is a quantification of the Loewe additivity method (36). CI was calculated for each of the twenty-five concentration points in which drugs were combined. We then assessed the distribution of levels where either synergy ($CI < 1$) or antagonism ($CI > 1$) was detected, broken by the diseases (Fig. 1B - 1C, Supplementary Table S2). Rather unexpectedly, we observed a notable variability between the tumor entities, with the highest overall rate of synergistic combinations in Ewing sarcoma.

Identification of a Ewing sarcoma specific synergy between PKC412 and IGF1R/INSR inhibitors

We sought for combinations that were specific and potent in Ewing sarcoma. To capture robust synergies, we compared the sums of concentration levels with a very strong synergy ($CI < 0.1$) for each drug pair, seeking for an unequal distribution across the three cancer entities (Fig 2A, Supplementary Table S2). Several drug-drug interactions proved to be specific for Ewing sarcoma (Fig. 2A, bars predominantly green, marked with asterisks). We hypothesized this to be a consequence of particular signaling alterations caused by EWS-FLI1, thus we used it as a starting point for a precision approach to target ES specific vulnerabilities. We investigated the known target spectra of the top six highly synergistic drug pairs and the database search results suggested that the crucial processes responsible for the strong inhibitory effect on cancer cell may be the obstruction of insulin and MAPK signaling, according to the KEGG database (Fig. 2B). PKC412, a staurosporine derivative annotated as a PKC/KIT inhibitor, showed considerable synergistic potential in Ewing sarcoma, as well as the both IGF1R inhibitors (BMS-754807 and OSI-906) represented in the library (Fig. 3A). A strong synergy between PKC412 and both IGF1R/INSR inhibitors ($CI < 0.1$) observed uniquely in the A673 cell line in up to 16 concentration points (concentration levels), was recapitulated in additional drug-drug matrices (Supplementary Fig. S2A). Moreover, the synergy was confirmed in a long-term assay where the combination efficiently inhibited the colony formation of A673 cells to a considerably larger extent than either of the drugs

alone (Fig. 3B). Annexin V immunostaining and subsequent flow cytometry analysis affirmed the increased frequency of dead and apoptotic cells in the combination treated sample (Fig. 3C) compared to the single drug effects, already after the 24 hours treatment. Next, we checked whether this potentiation is a consequence of alteration of either drug influx or drug efflux. Changes in the drug transport, however, did not account for the mechanism of synergy between PKC412 and BMS-754807, since neither of the drugs was interfering with the intracellular concentration of the other drug partner as shown by multiple reaction-monitoring assay (Supplementary Fig. S2B and S2C). Finally, we tested the combination in a panel of Ewing sarcoma cell lines that differed regarding sensitivity to single agents and expressed different forms of EWS-FLI1 fusion proteins (variations in the location of the *EWSR1* and *FLI-1* genomic breakpoints), and all of them displayed a comparable synergistic effect (Supplementary Table S3). We hypothesized that although high dose PKC412 may exert its effect on the transcriptional level, the crucial contribution to its synergy with IGF1R inhibitors may originate from the interference with signaling processes. We treated A673 cells with high-dose PKC412 (5 μ M), combination of inhibitors and single drugs at concentrations as in the combination, and measured mRNA levels of selected EWS-FLI1 regulated genes such as *NKX2-2*, *NR0B1* and *PHLDA1* (21,37,38). We compared it to the EWS-FLI1 knockdown (kd) sample, since the A673 cell line enables a conditional knockdown of EWS-FLI1 in a doxycycline dependent manner (39). PKC412 was shown to be a modulator of EWS-FLI1 target gene expression (21); however we observed only a modest EWS-FLI1 counterbalancing effect, and only upon high-dose PKC412 (Supplementary Fig. S3A). We observed a similar synergistic potential between PKC412 and both IGF1R/INSR inhibitors, indicating that the inhibition of the IGF1R axis is important and necessary for the synergy to occur. Upon stimulation with the IGF1R ligand IGF1, phosphorylation of the IGF1R and INSR and the downstream AKT signaling was impaired by BMS-754807 and the combination with PKC412; the same pattern was observed upon serum stimulation (Supplementary Fig. S3B). Further, PKC412 is a multi-targeted, promiscuous kinase inhibitor, recognized mostly for treatment of FLT3 mutated leukemia. FLT3 is poorly expressed in Ewing sarcoma and the target spectrum of PKC412 in this context was uncharted.

Conceptually straightforward approach to decipher the target profile of a drug is chemical proteomics, or drug pulldown (40). To elucidate the spectrum of proteins interacting with PKC412 in Ewing sarcoma cells we therefore applied the chemical proteomic approach (Fig. 3D). A coupleable analog of PKC412 (41) was immobilized on sepharose beads and affinity purification of interacting proteins from lysates of A673 cells was performed as described previously (26,41). To distinguish relevant targets in the Ewing sarcoma background, a reciprocal analysis with A673 cells upon EWS-FLI1 knockdown was performed. We assessed the temporal resolution of the knockdown

and selected the 72h time point as the best condition with a satisfying knockdown efficiency and minimal cellular senescence caused by EWS-FLI1 modulation (Fig. 4D). Although remnants of the fusion protein could still be detected at this time point, the overall presence and the impact of EWS-FLI1 were drastically impaired, thus allowing us to distinguish PKC412 targets greatly controlled by EWS-FLI1. Firstly, we checked whether doxycycline could impede the results and we confirmed that doxycycline does not chemically interfere with the other two compounds (data not shown). Low concentrations of tetracyclines inhibit mitochondrial function which could potentially confound experimental outcomes. When we checked in detail, however, none of the PKC412 targets we detected by chemoproteomics was found in the mitochondria-related gene expression datasets shown to be altered by doxycycline (42). Prior to LC-MS/MS analysis, drug pull-down samples from both A673 wt and EWS-FLI1 knockdown conditions were verified by immunoblotting for the presence of Aurora kinase A (AURKA), a known target of PKC412 and one of the kinases upregulated by the EWS-FLI1 oncoprotein (43). Although present in the lysates at a moderate level, AURKA was not detected in the pulldown experiment from EWS-FLI1 silenced cells (Supplementary Fig. S3C). Hence, we were able to confirm a differential target profile.

We computed the probability of true interaction using the SAINT algorithm (29) and opposed it to the magnitude of spectral count reduction upon competition with the free compound and we also considered the frequency of appearance in negative control experiments found in the CRAPome database (30). Altogether, this allowed us to capture the core target spectrum of PKC412 in Ewing sarcoma cell line (Fig. 3E). Interestingly, when we compared our results with the high confidence set of the drug-protein interactions reported in the computed STITCH database (44) for PKC412 we did not find a large overlap. This observation may not be surprising given the expected distinct mechanism of a drug in a particular EWS-FLI1 driven signaling context and the unbiased experimental nature of our approach. In agreement with the reported relative promiscuity of the drug, the target spectrum of PKC412 distributed across nearly the entire kinome evolutionary tree (Supplementary Fig. S3D). Almost the whole class of CAMKII kinases was captured in a complex with PKC412, as well as other cognate calcium signaling kinases, such as PRKCA, PRKCB and PDGFRB, arguing for a thorough blockade of the pathway (Fig. 3E). Interestingly, PDGFR is involved in mediating resistance to BMS-754807 in a human rhabdomyosarcoma model (45). We detected a number of high-confidence interactors that are related to insulin signaling according to the KEGG database (PDPK1, PRKAA2, PRKAB1, PRKAB2) (46). Moreover, PDPK1 can phosphorylate and activate AKT, allowing a cellular response to stimuli such as growth factors and insulin signaling. Overlap between the PI3K/AKT/mTOR and insulin pathways pointed to another interacting protein of PKC412, ULK3 (Unc-51 Like Kinase 3), a known regulator of autophagy, seemingly dependent on

EWS-FLI1 presence (Supplementary Fig. S3E). A number of the remaining PKC412 targets, such as FER, MAP/microtubule affinity-regulating kinase MARK2, discoidin domain receptor kinase DDR2, TBK1 and the interactor TANK, are also well-associated with the PI3K/AKT/mTOR pathway (47). Altogether, we concluded that PKC412 may exert its cytotoxic effect by inhibiting crucial Ewing sarcoma signaling routes – calcium, insulin and mTOR pathways. Moreover, we showed that the combination of PKC412 with an IGF1R/INSR inhibitor exhibited strong short- and long-term synergy in a broad range of concentrations and in a variety of Ewing sarcoma cell line model systems.

Quantitative phosphoproteomics identifies functionally relevant signaling networks altered by the drug combination in the context of Ewing sarcoma

Following up on the PKC412 target profiling, we set out to investigate the consequences of single and combinatorial drug treatment on the crucial signaling pathways. We compared three different conditions (PKC412 treated, BMS-754807 treated and combination treated A673 cells) to the DMSO treated A673 cells using a quantitative proteomics approach (48), where stable isotope labeling by amino acids in cell culture (SILAC) was combined with high-resolution liquid chromatography–tandem mass spectrometry (LC-MS/MS) (experimental overview given in Supplementary Fig. S4A). The numbers of identified phosphosites were in agreement with previous studies (32,49) and different drug treatments displayed a good reproducibility with a Pearson correlation R in the range of 0.62-0.82 (Supplementary Fig. S4B and S4C). As expected, the majority of phosphorylation sites regulated by single drugs were overlapping with the combination treatment. Out of 667 sites downregulated by the combination, more than half (386) were uniquely altered by the combination (Fig. 4A). The same was evident with the compound-induced upregulation of phosphorylation sites (Fig. 4A), arguing for the exclusive mechanism of the combined effect. Phosphorylation site changes were visualized by hierarchical clustering, where we implemented a cluster-dependent sequence motif enrichment analysis of the phosphorylation sites and observed a strong preference for PKC/AKT and MAPK motifs (Fig. 4B). Interestingly, an ATM/ATR motif was upregulated by PKC412 and the combinatorial treatment, possibly due to the activation of stress related DNA damage inducing pathways. The overall effect of the combinatorial treatment that we observed was truly synergistic in nature, since it encompassed single effects of both of the drugs and supplemented an additional combinatorial response that was distinct from the overlap of the single drugs effect and resulted in an additional alternation of core signaling processes. KEGG pathway enrichment analysis suggested the MAPK pathway, mTOR signaling, and the insulin pathway as some of the of sites downregulated specifically by combination. (Supplementary Fig. S4D, Supplementary Fig. S5). In

concordance with the PKC412 chemical proteomic data, the combination treatment indicated an overrepresentation of PKA and CaMKII motifs for downregulated sites (Supplementary Fig. S4E). For a number of relevant phosphoproteins we observed a considerably stronger downregulation when drugs were applied together compared to PKC412 alone at the same concentration. For instance, this held true for a number of Ca²⁺/calmodulin dependent kinases (CAMK2D, DAPK2, CAMK1, PRKCB). Some of those have been shown to be PKC412 targets but the overall effect was decidedly potentiated by the second drug. Since the cluster-dependent sequence motif analysis of the phosphorylation sites pointed to a preference for AKT, MAPK and ERK1/2 (extracellular-signal-regulated kinases), we checked it in more detail.

Similarly to rapamycin (mTORC1 inhibitor) and torin (dual mTORC1 and mTORC2 inhibitor) the PKC412/BMS-754807 combination inhibited activation of the mTOR pathway, demonstrated by its hallmark phosphorylation of a downstream TORC1 effector p70S6 kinase (S6K) at the threonine residue 389 (T389) (Fig. 4C). The effect of the combination was considerably stronger than the effect of either of the drugs alone. As an mTORC1 inhibitor, rapamycin failed to down-regulate TORC2 dependent AKT phosphorylation on serine 473 (S473), while this phosphorylation site was strongly inhibited by torin and, notably, by the synergistic combination. Moreover, both mTOR inhibitors induced the suppression of a negative feedback loop, which leads to the AKT pathway stimulation and subsequent cell survival (50), identified through phosphorylation on the catalytic site for AKT activation, threonine 308 (T308). Importantly, this compensatory re-activation was not induced by the PKC412/IGF1R inhibitor combination; on the contrary, combination treatment caused potent inhibition of T308 AKT phosphorylation. Rewiring of signaling networks was hence circumvented, a notion strengthened by the observed inhibition of the ERK1/p44 and ERK2/p42 activation by the combination, although seen intermittently (Fig. 4C and Supplementary Fig. S4F). This argued for an exhaustive impairment of the cross-talk between various pro-survival pathways. Identical series of signaling inhibition was observed when OSI-906, another IGF1R/INSR inhibitor, was used instead of BMS-754807 in combination with PKC412 (Supplementary Fig. S4F). Finally, to check for EWS-FLI1 dependence, we performed the knockdown of EWS-FLI1 in the A673 cell line (Fig. 4D) and assessed the profile of signaling changes after 72h upon the knockdown induction (Fig. 4E). While the mTOR inhibitors exhibited an identical pattern as in the wild type cells, the PKC412/BMS-754807 combination treatment was suddenly ineffective, demonstrating the dependency of the effect to the EWS-FLI1 altered signaling. Similar pattern of signaling events as in A673 cells we observed in additional Ewing sarcoma cell lines, TC71 and TC252 (Fig. 4F), while the combination was ineffective in the two non-Ewing cell lines, medulloblastoma UW228 and

neuroblastoma IMR5-75 cells, although mTOR inhibitors were still effective (Fig. 4G). We concluded that the overall effect of the combinatorial treatment is the consequence of an exclusive combinatorial response that resulted in thorough alteration of core signaling processes determined by EWS-FLI1 and important for the Ewing sarcoma tumor survival and progression.

Discussion

Resistance to targeted agents occurs frequently and poses a major limitation in clinical practice. It can be caused by various molecular mechanisms that cancer cells adopt when challenged with small molecule drugs for prolonged periods (51,52). Compensatory pathways can remodel the signaling landscape and cause drug ineffectiveness (53). However, synergistic activity of two drugs with distinct primary mechanism of action, can improve treatment efficacy, especially in complex diseases where the control is more likely to be accomplished by using multiple interventions (54,55). By charting disease specific functional synergies onto pathways, we aimed to decipher synergistic signaling cross-talks in a particular Ewing sarcoma context. We observed a strong synergistic potential of PKC412 specifically in the Ewing sarcoma combinatorial screen, notably with IGF1R/INSR inhibitors. Target spectrum analysis of PKC412 in Ewing sarcoma revealed that in the absence of its main cognate targets (56) and in a particular signaling background directed by the fusion oncoprotein EWS-FLI1, PKC412 exhibited its cytotoxic effect primarily by suppression of signaling routes that appeared to be the most prominent in Ewing sarcoma: the PI3K/AKT/mTOR, insulin and calcium/calmodulin signaling axes (17). IGF1R inhibitors, both antibody-based and small molecules, are considered an exciting option in precision medicine-based Ewing sarcoma treatment, since IGF1 signaling is known to be heavily altered in Ewing sarcoma due to a number of related EWS-FLI1 target genes (15). Yet, it proved to be difficult to identify patients that would benefit from the therapy and even in responsive patients resistance occurred frequently (16,57). Combination of PKC412 with the two IGF1R/INSR small molecule inhibitors was consistently and strongly synergistic in a panel of assorted Ewing sarcoma cell lines, while mild antagonism or additivity was observed in parallel screens in neuroblastoma and medulloblastoma. Advantageously for a possible therapeutic application, the effect was spread across a broad range of concentrations, arguing for a potentially wide application. Mechanistically, the combination triggered a different array of responses in cancer cells compared to a single drug treatment. A significant portion of

regulated phosphorylated sites was found to be unique for the combination treatment, strongly arguing that the combined effect was more than a simple sum of the individual events. A coordinated inhibition of AKT/PI3K/mTOR and MAPK signaling pathways was considerably stronger by the combination than by either of the drugs alone. Importantly, this effect was EWS-FLI1 dependent, unlike in case of mTOR inhibitors. Moreover, compensatory suppression of the negative feedback loops was surpassed by the simultaneous application PKC412 and the IGF1R/INSR inhibitor, potentially leading to overcoming the resistance. The reduced dosing enabled by the synergistic effect would lessen the associated adverse side effects, which is particularly important in pediatric tumors where patients experience long-term treatment consequences. The Ewing sarcoma-specific combinations of targeted agents that we identified have the potential to be readily translated into clinical treatment. This is particularly important as improvements in survival for Ewing sarcoma patients have been modest. We paved the way for *in-silico* synergy modeling by mapping chemical perturbations in three pediatric tumors in a comparable manner, which can also allow for a better understanding of the complex disease system itself.

References

1. Gorlick R, Janeway K, Lessnick S, Randall RL, Marina N, Committee on behalf of the COGBT. Children's Oncology Group's 2013 blueprint for research: Bone tumors. *Pediatr Blood Cancer*. 2013;60:1009–15.
2. Smith MA, Seibel NL, Altekruse SF, Ries LAG, Melbert DL, O'Leary M, et al. Outcomes for Children and Adolescents With Cancer: Challenges for the Twenty-First Century. *J Clin Oncol*. 2010;28:2625–34.
3. Crompton BD, Stewart C, Taylor-Weiner A, Alexe G, Kurek KC, Calicchio ML, et al. The Genomic Landscape of Pediatric Ewing Sarcoma. *Cancer Discov*. 2014;4:1326–41.
4. Delattre O, Zucman J, Plougastel B, Desmaze C, Melot T, Peter M, et al. Gene fusion with an ETS DNA-binding domain caused by chromosome translocation in human tumours. *Nature*. 1992;359:162–5.
5. May WA, Lessnick SL, Braun BS, Klemsz M, Lewis BC, Lunsford LB, et al. The Ewing's sarcoma EWS/FLI-1 fusion gene encodes a more potent transcriptional activator and is a more powerful transforming gene than FLI-1. *Mol Cell Biol*. 1993;13:7393–8.
6. Tirode F, Surdez D, Ma X, Parker M, Le Deley MC, Bahrami A, et al. Genomic Landscape of Ewing Sarcoma Defines an Aggressive Subtype with Co-Association of STAG2 and TP53 Mutations. *Cancer Discov*. 2014;4:1342–53.
7. Brohl AS, Solomon DA, Chang W, Wang J, Song Y, Sindiri S, et al. The Genomic Landscape of the Ewing Sarcoma Family of Tumors Reveals Recurrent STAG2 Mutation. *PLoS Genet*. 2014;10:e1004475.
8. Lerman DM, Monument MJ, McIlvaine E, Liu X, Huang D, Monovich L, et al. Tumoral TP53 and/or CDKN2A alterations are not reliable prognostic biomarkers in patients with localized Ewing sarcoma: A report from the Children's Oncology Group. *Pediatr Blood Cancer*. 2015;62:759–65.
9. Herrero-Martin D, Fourtouna A, Niedan S, Riedmann LT, Schwentner R, Aryee DNT. Factors Affecting EWS-FLI1 Activity in Ewing's Sarcoma. *Sarcoma*. 2011;2011:352580.
10. Bailly RA, Bosselut R, Zucman J, Cormier F, Delattre O, Roussel M, et al. DNA-binding and transcriptional activation properties of the EWS-FLI-1 fusion protein resulting from the t(11;22) translocation in Ewing sarcoma. *Mol Cell Biol*. 1994;14:3230–41.
11. Schwentner R, Papamarkou T, Kauer MO, Stathopoulos V, Yang F, Bilke S, et al. EWS-FLI1 employs an E2F switch to drive target gene expression. *Nucleic Acids Res*. 2015;43:2780–9.
12. Potratz J, Tillmanns A, Berning P, Korsching E, Schaefer C, Lechtape B, et al. Receptor tyrosine kinase gene expression profiles of Ewing sarcomas reveal ROR1 as a potential therapeutic target in metastatic disease. *Mol Oncol*. 2016;10:677–92.
13. Scotlandi K, Benini S, Sarti M, Serra M, Lollini P-L, Maurici D, et al. Insulin-like Growth Factor I Receptor-mediated Circuit in Ewing's Sarcoma/Peripheral Neuroectodermal Tumor: A Possible Therapeutic Target. *Cancer Res*. 1996;56(20):4570–4.
14. Toretsky JA, Kalebic T, Blakesley V, LeRoith D, Helman LJ. The Insulin-like Growth Factor-I Receptor Is Required for EWS/FLI-1 Transformation of Fibroblasts. *J Biol Chem*. 1997;272(49):30822–7.
15. Cironi L, Riggi N, Provero P, Wolf N, Suvà M-L, Suvà D, et al. IGF1 Is a Common Target Gene of Ewing's Sarcoma Fusion Proteins in Mesenchymal Progenitor Cells. *PLoS One*. 2008;3(7):e2634.
16. Naing A, LoRusso P, Fu S, Hong DS, Anderson P, Benjamin RS, et al. Insulin Growth

- Factor-Receptor (IGF-1R) Antibody Cixutumumab Combined with the mTOR Inhibitor Temsirolimus in Patients with Refractory Ewing's Sarcoma Family Tumors. *Clin Cancer Res.* 2012;18(9):2625–31.
17. Toretzky JA, Thakar M, Eskenazi AE, Frantz CN. Phosphoinositide 3-Hydroxide Kinase Blockade Enhances Apoptosis in the Ewing's Sarcoma Family of Tumors. *Cancer Res.* 1999;59(22):5745–50.
 18. Samatar AA, Poulikakos PI. Targeting RAS-ERK signalling in cancer: promises and challenges. *Nat Rev Drug Discov.* 2014;13(12):928–42.
 19. Jiang Y, Ludwig J, Janku F. Targeted therapies for advanced Ewing sarcoma family of tumors. *Cancer Treat Rev.* 2015;41(5):391–400.
 20. Greco WR, Bravo G, Parsons JC. The search for synergy: a critical review from a response surface perspective. *Pharmacol Rev.* 1995;47(2):331–85.
 21. Boro A, Prêtre K, Rechfeld F, Thalhammer V, Oesch S, Wachtel M, et al. Small-molecule screen identifies modulators of EWS/FLI1 target gene expression and cell survival in Ewing's sarcoma. *Int J Cancer.* 2012;131(9):2153–64.
 22. Avnet S, Sciacca L, Salerno M, Gancitano G, Cassarino MF, Longhi A, et al. Insulin Receptor Isoform A and Insulin-like Growth Factor II as Additional Treatment Targets in Human Osteosarcoma. *Cancer Res.* 2009;69(6):2443–52.
 23. Chen HX, Sharon E. IGF-1R as an anti-cancer target—trials and tribulations. *Chin J Cancer.* 2013;32(5):242–52.
 24. Chou T-C. Theoretical Basis, Experimental Design, and Computerized Simulation of Synergism and Antagonism in Drug Combination Studies. *Pharmacol Rev.* 2006;58(3):621–81.
 25. Rix U, Hantschel O, Dürnberger G, Remsing Rix LL, Planyavsky M, Fernbach N V, et al. Chemical proteomic profiles of the BCR-ABL inhibitors imatinib, nilotinib, and dasatinib reveal novel kinase and nonkinase targets. *Blood.* 2007;110(12):4055–63.
 26. Radic-Sarikas B, Rix U, Stukalov A, Gridling M, Müller AC, Colinge J, et al. Enhancing cognate target elution efficiency in gel-free chemical proteomics. *EuPA Open Proteomics.* 2015;9:43–53.
 27. Maurer M, Müller AC, Wagner C, Huber ML, Rudashevskaya EL, Wagner SN, et al. Combining Filter-Aided Sample Preparation and Pseudoshotgun Technology To Profile the Proteome of a Low Number of Early Passage Human Melanoma Cells. *J Proteome Res.* 2013;12:1040–8.
 28. Kersey P, Hermjakob H, Apweiler R. VARSPLIC: alternatively-spliced protein sequences derived from SWISS-PROT and TrEMBL. *Bioinformatics.* 2000;16:1048–9.
 29. Choi H, Larsen B, Lin Z-Y, Breitkreutz A, Mellacheruvu D, Fermin D, et al. SAINT: probabilistic scoring of affinity purification-mass spectrometry data. *Nat Meth.* 2011;8:70–3.
 30. Mellacheruvu D, Wright Z, Couzens AL, Lambert J-P, St-Denis NA, Li T, et al. The CRAPome: a contaminant repository for affinity purification-mass spectrometry data. *Nat Meth.* 2013;10:730–6.
 31. Batth TS, Francavilla C, Olsen J V. Off-Line High-pH Reversed-Phase Fractionation for In-Depth Phosphoproteomics. *J Proteome Res.* 2014;13:6176–86.
 32. Olsen J V., Blagoev B, Gnad F, Macek B, Kumar C, Mortensen P, et al. Global, In Vivo, and Site-Specific Phosphorylation Dynamics in Signaling Networks. *Cell.* 2006;127:635–48.
 33. Cox J, Mann M. MaxQuant enables high peptide identification rates, individualized p.p.b.-

- range mass accuracies and proteome-wide protein quantification. *Nat Biotech.* 2008;26:1367–72.
34. Lehár J, Stockwell BR, Giaever G, Nislow C. Combination chemical genetics. *Nat Chem Biol.* 2008;4:674–81.
 35. Chou TC, Talalay P. Quantitative analysis of dose-effect relationships: the combined effects of multiple drugs or enzyme inhibitors. *Adv Enzyme Regul.* 1984;22:27–55.
 36. Loewe S, Muischnek H. Über Kombinationswirkungen. *Naunyn Schmiedebergs Arch Exp Pathol Pharmacol.* 1926;114:313–26.
 37. Smith R, Owen LA, Trem DJ, Wong JS, Whangbo JS, Golub TR, et al. Expression profiling of EWS/FLI identifies NKX2.2 as a critical target gene in Ewing's sarcoma. *Cancer Cell.* 2006;9:405–16.
 38. Kinsey M, Smith R, Lessnick SL. NR0B1 Is Required for the Oncogenic Phenotype Mediated by EWS/FLI in Ewing's Sarcoma. *Mol Cancer Res.* 2006;4:851–9.
 39. Carrillo J, García-Aragoncillo E, Azorín D, Agra N, Sastre A, González-Mediero I, et al. Cholecystokinin Down-Regulation by RNA Interference Impairs Ewing Tumor Growth. *Clin Cancer Res.* 2007;13:2429–40.
 40. Rix U, Superti-Furga G. Target profiling of small molecules by chemical proteomics. *Nat Chem Biol.* 2009;5:616–24.
 41. Borgdorff V, Rix U, Winter GE, Gridling M, Muller AC, Breitwieser FP, et al. A chemical biology approach identifies AMPK as a modulator of melanoma oncogene MITF. *Oncogene.* 2014;33:2531–9.
 42. Moullan N, Mouchiroud L, Wang X, Ryu D, Williams EG, Mottis A, et al. Tetracyclines disturb mitochondrial function across eukaryotic models: A call for caution in biomedical research. *Cell Rep.* 2015;10:1681–91.
 43. Winter GE, Rix U, Lissat A, Stukalov A, Müllner MK, Bennett KL, et al. An Integrated Chemical Biology Approach Identifies Specific Vulnerability of Ewing's Sarcoma to Combined Inhibition of Aurora Kinases A and B. *Mol Cancer Ther.* 2011;10:1846–56.
 44. Kuhn M, von Mering C, Campillos M, Jensen LJ, Bork P. STITCH: interaction networks of chemicals and proteins. *Nucleic Acids Res.* 2008;36:D684–8.
 45. Huang F, Hurlburt W, Greer A, Reeves KA, Hillerman S, Chang H, et al. Differential Mechanisms of Acquired Resistance to Insulin-like Growth Factor-I Receptor Antibody Therapy or to a Small-Molecule Inhibitor, BMS-754807, in a Human Rhabdomyosarcoma Model. *Cancer Res.* 2010;70:7221–31.
 46. Davis MI, Hunt JP, Herrgard S, Ciceri P, Wodicka LM, Pallares G, et al. Comprehensive analysis of kinase inhibitor selectivity. *Nat Biotechnol.* 2011;29:1046–51.
 47. Ou Y-H, Torres M, Ram R, Formstecher E, Roland C, Cheng T, et al. TBK1 directly engages Akt/PKB survival signaling to support oncogenic transformation. *Mol Cell.* 2011;41:458–70.
 48. Olsen J V, Mann M. Status of Large-scale Analysis of Post-translational Modifications by Mass Spectrometry. *Mol Cell Proteomics.* 2013;12:3444–52.
 49. Emdal KB, Pedersen A-K, Bekker-Jensen DB, Tsafou KP, Horn H, Lindner S, et al. Temporal proteomics of NGF-TrkA signaling identifies an inhibitory role for the E3 ligase Cbl-b in neuroblastoma cell differentiation. *Sci Signal.* 2015;8:ra40-ra40.
 50. Peterson TR, Laplante M, Thoreen CC, Sancak Y, Kang SA, Kuehl WM, et al. DEPTOR Is an mTOR Inhibitor Frequently Overexpressed in Multiple Myeloma Cells and Required for Their Survival. *Cell.* 2009;137:873–86.
 51. Groenendijk FH, Bernards R. Drug resistance to targeted therapies: déjà vu all over again.

- Mol Oncol. 2014;8:1067–83.
52. Wood KC. Mapping the Pathways of Resistance to Targeted Therapies. *Cancer Res.* 2015;75:4247–51.
 53. Rozengurt E, Soares HP, Sinnet-Smith J. Suppression of feedback loops mediated by PI3K/mTOR induces multiple overactivation of compensatory pathways: an unintended consequence leading to drug resistance. *Mol Cancer Ther.* 2014;13:2477–88.
 54. Feala JD, Cortes J, Duxbury PM, Piermarocchi C, McCulloch AD, Paternostro G. Systems approaches and algorithms for discovery of combinatorial therapies. *Wiley Interdiscip Rev Syst Biol Med.* 2010;2:181–93.
 55. Wildenhain J, Spitzer M, Dolma S, Jarvik N, White R, Roy M, et al. Prediction of Synergism from Chemical-Genetic Interactions by Machine Learning. *Cell Syst.* 2016;1:383–95.
 56. Peter B, Winter GE, Blatt K, Bennett KL, Stefanzi G, Rix U, et al. Target interaction profiling of midostaurin and its metabolites in neoplastic mast cells predicts distinct effects on activation and growth. *Leukemia.* 2016;30:464–72.
 57. Arnaldez FI, Helman LJ. New strategies in ewing sarcoma: lost in translation? *Clin Cancer Res.* 2014;20:3050–6.

Acknowledgements

We thank Georg Winter, Uwe Rix, Claudia Trefzer, Eleni Tomazou, Konstantinos Papakostas, Johannes Bigenzahn, Dorte B. Bekker-Jensen, Anna-Kathrine Pedersen and Dave Aryee for skillful advice and help. We also want to thank for the generous gifts of cell lines or reagents, Alexandre Arcaro, Javier Alonso, and Frank Westermann.

Data and materials availability:

The raw MS data and associated tables have been deposited to the ProteomeXchange Consortium via the PRIDE partner repository with the data set identifier PXD002765 (<http://proteomecentral.proteomexchange.org>).

Figure legends

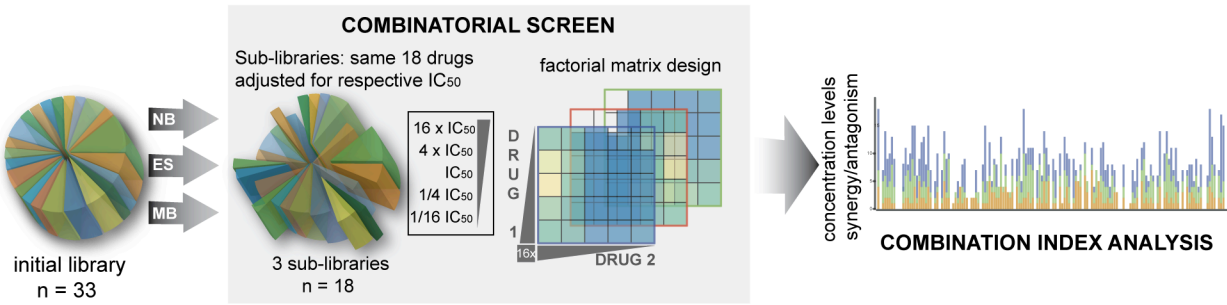
Fig. 1. Drug-drug interactions identified in combinatorial drug screens in the three pediatric tumor cell lines. (A) Workflow of a dilution-matrix based parallel combinatorial screens in the three pediatric tumor entities. (B) Distribution of synergy across the three screens; shown is a number of concentration levels where for each cell line $CI < 1$ and $CI > 1$ in the remaining two cell lines. The drug pair was concealed in cases $CI = 0$ or when CI was not calculable. Blue, neuroblastoma; green, Ewing sarcoma; red, medulloblastoma. (C) Distribution of antagonism across the three tumor entities; shown is a number of concentration levels where in each cell line $CI > 1$ and $CI < 1$ in the remaining two cell lines. The drug pair was concealed in cases $CI=0$ or when CI was not calculable. Blue, neuroblastoma; green, Ewing sarcoma; red, medulloblastoma.

Fig. 2. Ewing sarcoma-specific synergies converge around same signaling axes. (A) Distribution of very strong synergy ($CI < 0.1$) across concentration levels in the three pediatric tumor entities. Shown is a number of concentration levels where for each cell line $CI < 0.1$ and $CI > 1$ in the remaining two cell lines. Blue, neuroblastoma; green, Ewing sarcoma; red, medulloblastoma. Six pairs with the strongest Ewing sarcoma-specific synergistic effect are emboldened in black and marked with stars. (B) Network representing targets of the six most prominent Ewing sarcoma specific synergistic drug pairs. Affected processes are outlined, according to the KEGG database.

Fig. 3. Interaction between PKC412 and IGF1R/INSR inhibitors is synergistic in Ewing sarcoma. (A) Chemical structures of PKC412 and the two IGF1R inhibitors from the panel, OSI-906 and BMS-754807. (B) Colony formation assay. PKC412 (red border) was used at 0.25 IC50 concentration (75 nM), BMS-754807 (green border) at 0.25 IC50 (18 nM). DMSO (grey border) treated cells were used as a control. Data shown as mean \pm s.e.m. and images are representative of triplicate experiments ($P < 0.05$, t-test). (C) AnnexinV/DAPI staining of A673 cells after 24 h of compound treatment with PKC412 at 150 nM (0.5 IC50) and BMS-754807 at 35 nM (0.5 IC50). The percentage of apoptotic, dead, and alive cells was determined and data are shown as means \pm s.d. from three independent experiments. (D) Schematic of the chemical proteomic workflow. (E) Results from mass-spectrometry-based proteomic affinity purification experiment using competition analysis and SAINT. Data shown are based on two independent experiments for each condition (A673 cell lysate and A673 lysate pretreated with the free drug, i.e. competition pull-down); each biological replicate was analyzed in two technical replicates.

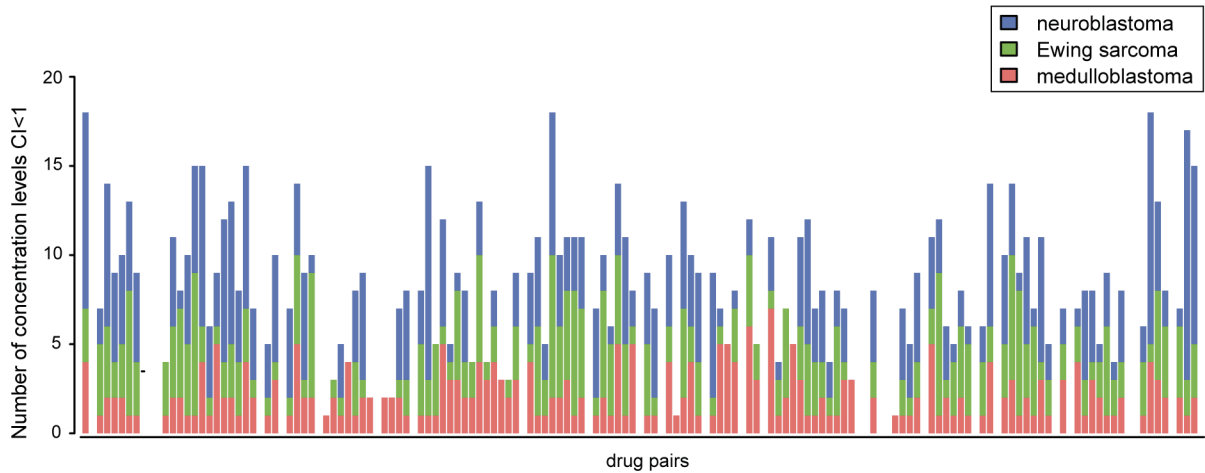
Fig. 4. Quantitative phosphoproteomics identifies PKC/AKT/mTOR and MAPK signaling networks as functionally relevant for the synergistic effect of the drug combination. (A) Overlap of altered phosphorylation sites upon single drugs and combinatorial treatment. (B) Hierarchical clustering of phosphorylation site changes including cluster-dependent sequence motif enrichment analysis of the phosphorylation sites. (C) Immunoblots showing changes in phosphorylation of representative PKC/AKT/mTOR and MAPK kinases after combinatorial drug treatment. Cells were starved overnight, treated as indicated for 2h and stimulated with serum for 20 minutes. Treatment doses: PKC412: 75 nM ($\frac{1}{4}$ IC50); BMS754807: 18 nM ($\frac{1}{4}$ IC50); combination: concurrently 75 nM PKC412 and 18 nM BMS754807; torin: 250 nM; rapamycin: 1 μ M. (D) Temporal resolution of the EWS-FLI1 knockdown. 72h time point was selected for the chemical proteomic and immunoblot experiment. (E) Immunoblot showing changes in phosphorylation upon drug treatment when EWS-FLI1 knockdown was induced. At the 72h doxycyclin induction time point the cells were starved overnight, treated as indicated for 2h and stimulated with serum for 20 minutes. Treatment doses: PKC412: 75 nM ($\frac{1}{4}$ IC50); BMS754807: 18nM ($\frac{1}{4}$ IC50); combination: concurrently 75 nM PKC412 and 18 nM BMS754807; torin: 250 nM; rapamycin: 1 μ M. (F) Immunoblots upon drug treatment in additional Ewing sarcoma cell lines TC71 and TC252. Cells were starved overnight, treated as indicated for 2h and stimulated with serum for 20 minutes. Treatment doses: PKC412: $\frac{1}{4}$ IC50 (1100 nM in TC71, 10.5 nM in TC252); BMS754807: $\frac{1}{4}$ IC50 (320 nM in TC71, 8.5 nM in TC252); combination: concurrently $\frac{1}{4}$ IC50 PKC412 and $\frac{1}{4}$ IC50 BMS754807; torin: 250 nM; rapamycin: 1 μ M. n=2. (G) Immunoblots upon drug treatment in additional non-Ewing sarcoma cell lines, UW228 (medulloblastoma) and IMR5-75 (neuroblastoma). Cells were starved overnight, treated as indicated for 2h and stimulated with serum for 20 minutes. Treatment doses: PKC412: $\frac{1}{4}$ IC50 (125 nM in UW228, 36 nM in IMR5-75); BMS754807: $\frac{1}{4}$ IC50 (250 nM in UW228, 96 nM in IMR5-75); combination: concurrently $\frac{1}{4}$ IC50 PKC412 and $\frac{1}{4}$ IC50 BMS754807; torin: 250 nM; rapamycin: 1 μ M.

A



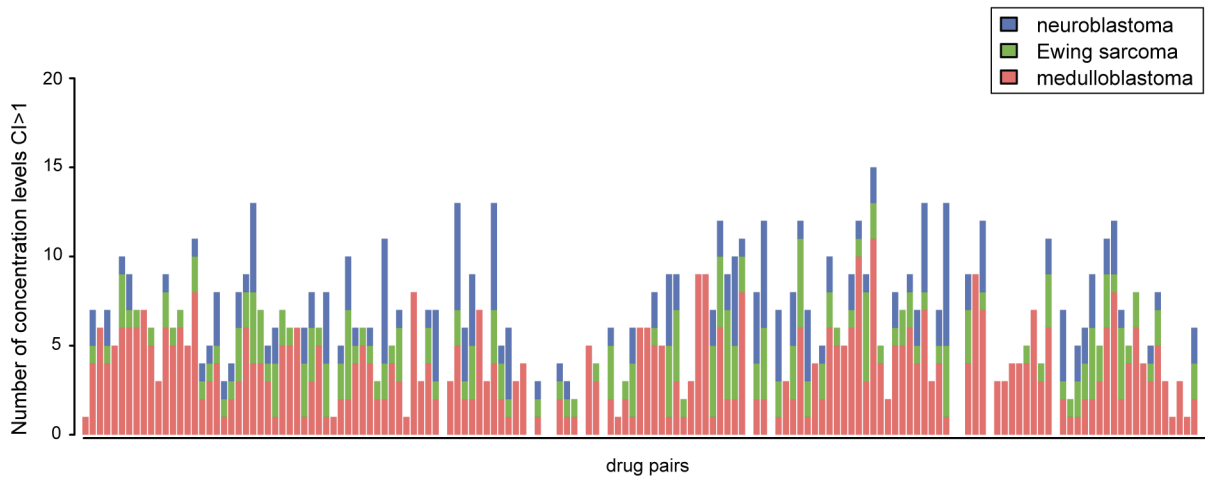
B

Distribution of drug synergy across combinatorial screens



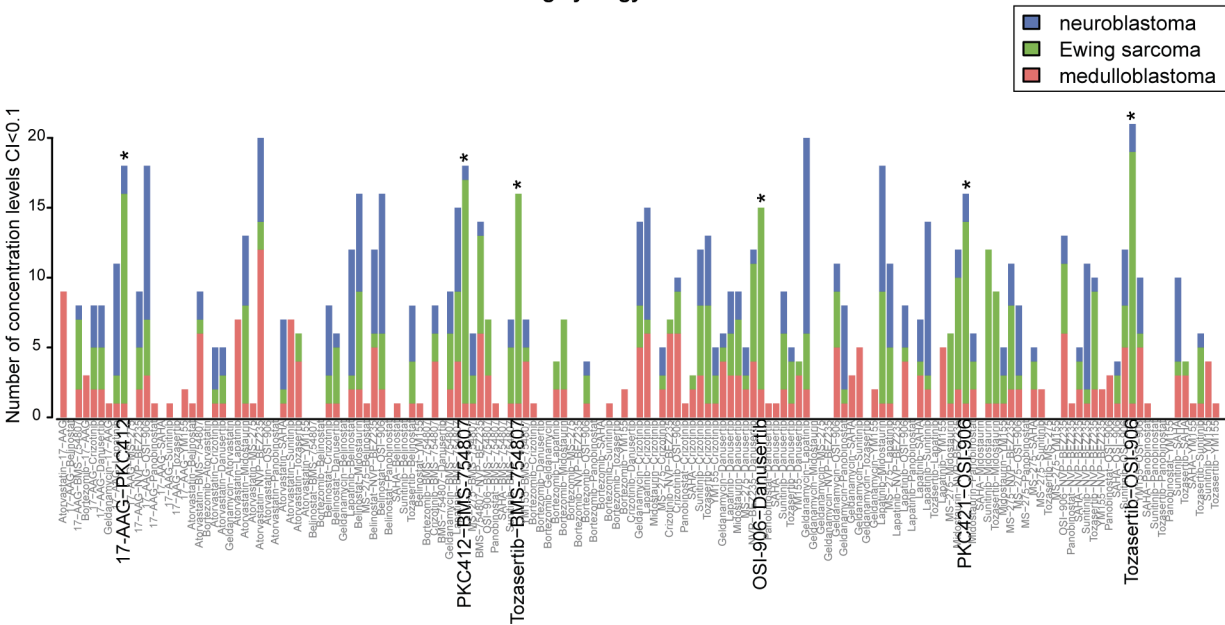
C

Distribution of drug antagonism across combinatorial screens



A

Distribution of strong synergy across combinatorial screens



B

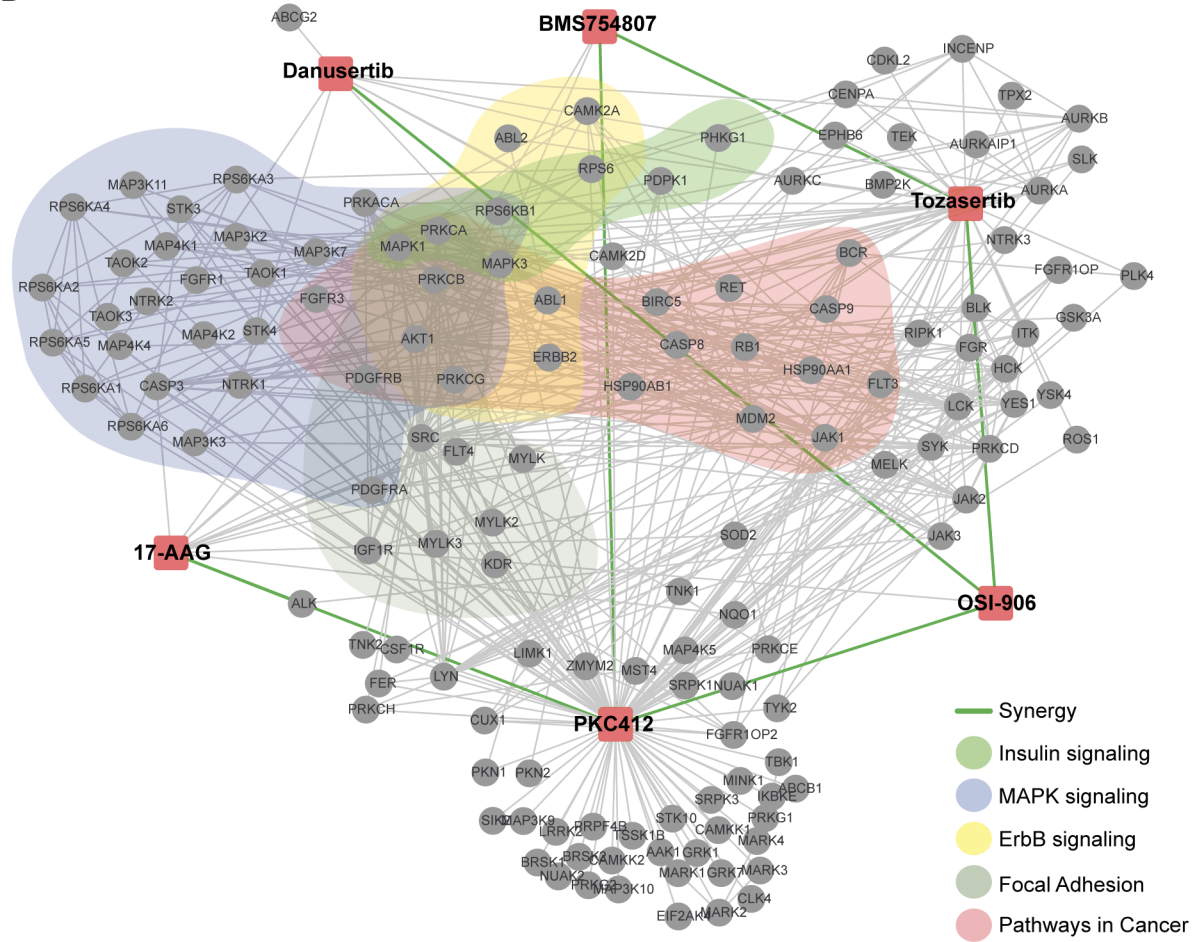
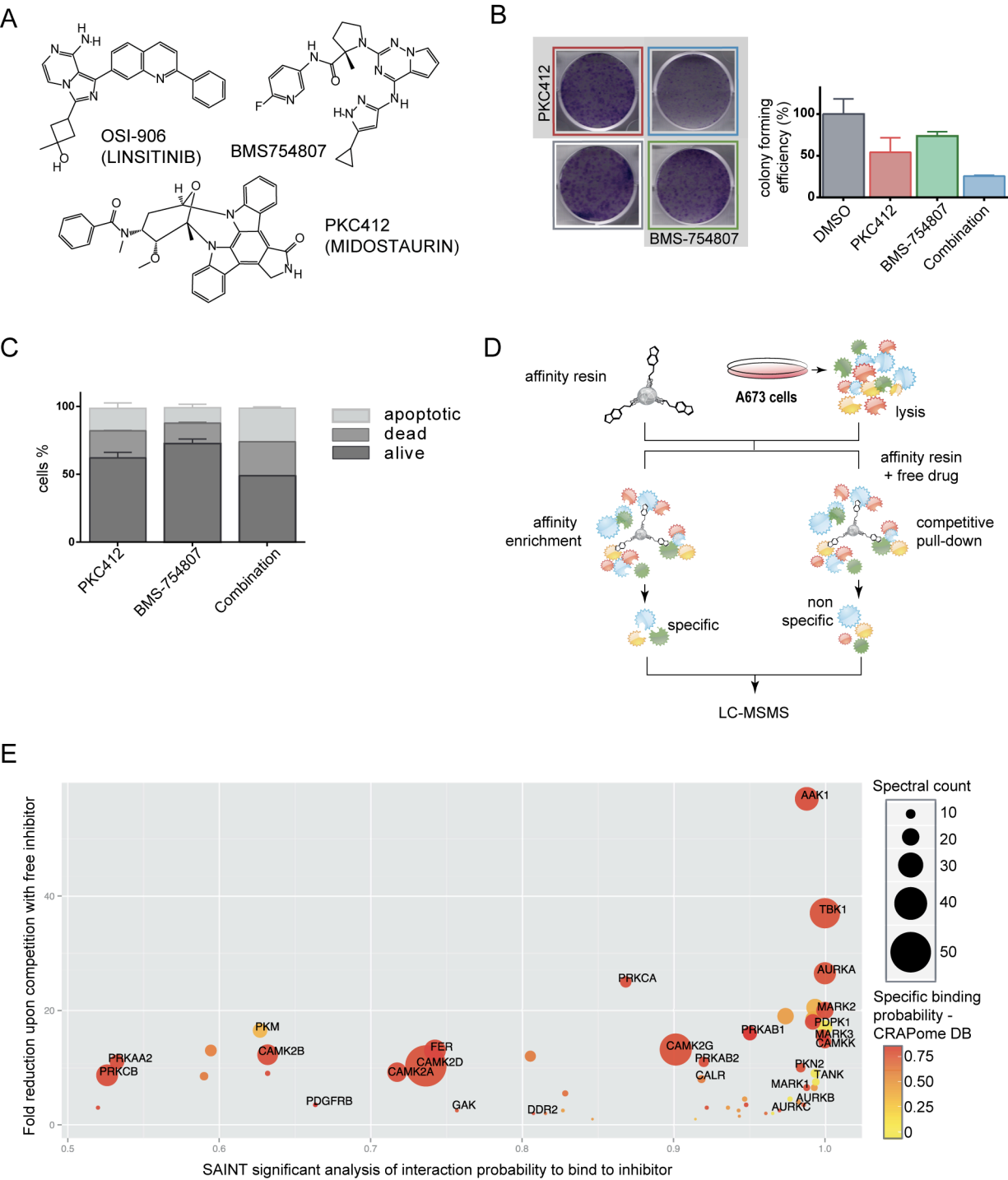
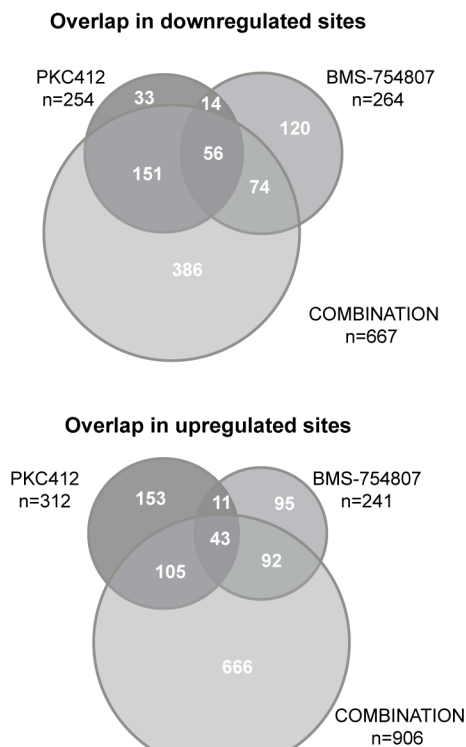


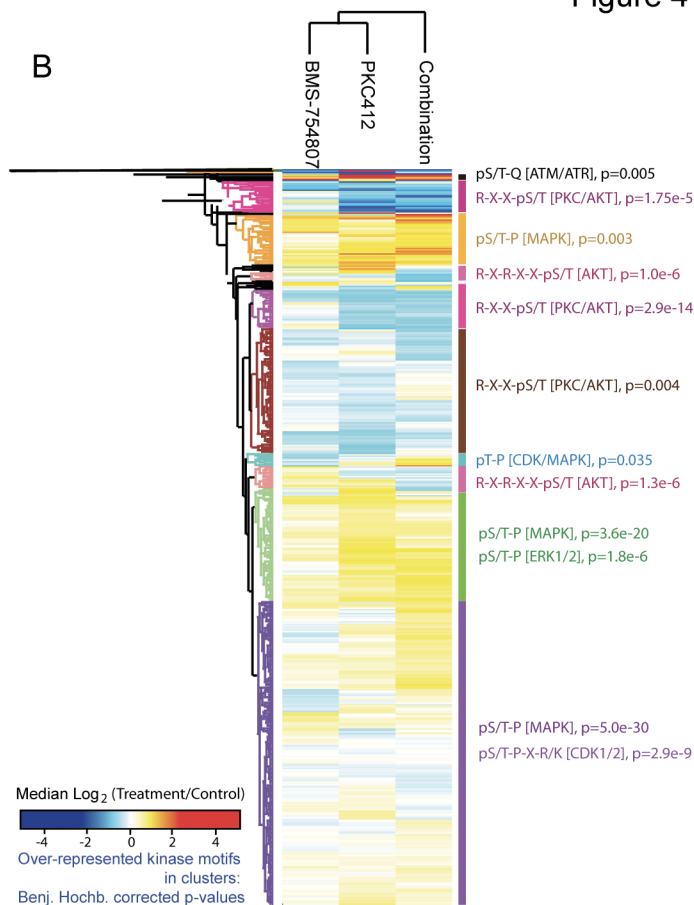
Figure 3



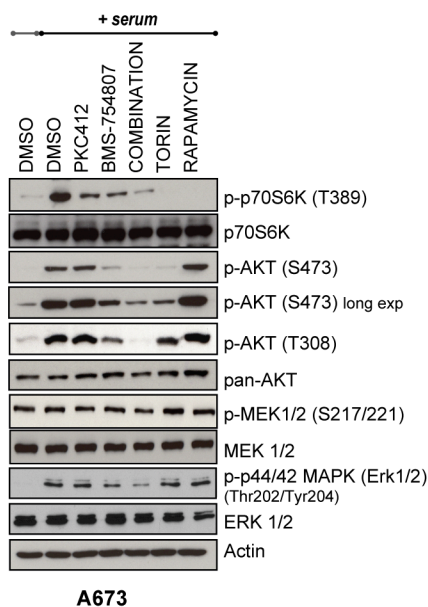
A



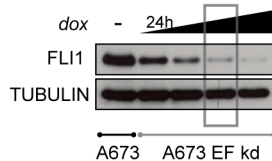
B



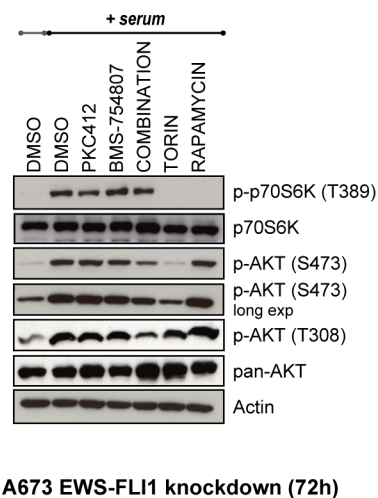
C



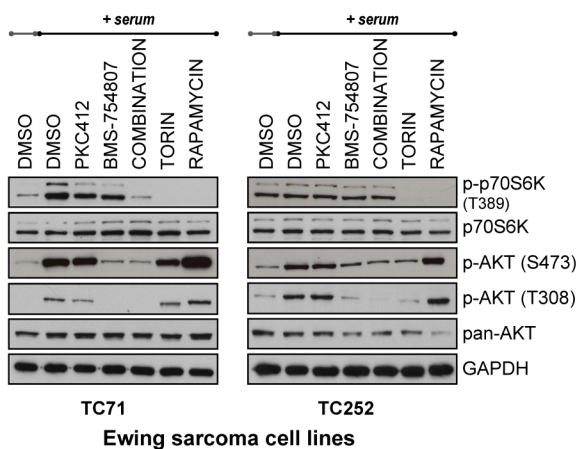
D



E



F



G

